

Multiview hyperspectral topography of tissue structural and functional characteristics

Shiwu Zhang^{a,b}, Peng Liu^a, Jiwei Huang^b, Ronald Xu^{a,b}

^aDepartment of Precision Machinery and Precision Instrumentation, University of Science and Technology of China, Hefei, China, 230027

^bDepartment of Biomedical Engineering, The Ohio State University, Columbus, OH 43210

ABSTRACT

Accurate and in vivo characterization of structural, functional, and molecular characteristics of biological tissue will facilitate quantitative diagnosis, therapeutic guidance, and outcome assessment in many clinical applications, such as wound healing, cancer surgery, and organ transplantation. However, many clinical imaging systems have limitations and fail to provide noninvasive, real time, and quantitative assessment of biological tissue in an operation room. To overcome these limitations, we developed and tested a multiview hyperspectral imaging system. The multiview hyperspectral imaging system integrated the multiview and the hyperspectral imaging techniques in a single portable unit. Four plane mirrors are cohered together as a multiview reflective mirror set with a rectangular cross section. The multiview reflective mirror set was placed between a hyperspectral camera and the measured biological tissue. For a single image acquisition task, a hyperspectral data cube with five views was obtained. The five-view hyperspectral image consisted of a main objective image and four reflective images. Three-dimensional topography of the scene was achieved by correlating the matching pixels between the objective image and the reflective images. Three-dimensional mapping of tissue oxygenation was achieved using a hyperspectral oxygenation algorithm. The multiview hyperspectral imaging technique is currently under quantitative validation in a wound model, a tissue-simulating blood phantom, and an in vivo biological tissue model. The preliminary results have demonstrated the technical feasibility of using multiview hyperspectral imaging for three-dimensional topography of tissue functional properties.

Keywords: multi-view, hyperspectral, oxygenation, topography, reconstruction.

1. INTRODUCTION

Accurate and in vivo characterization of structural, functional, and molecular characteristics of biological tissue will facilitate quantitative diagnosis, therapeutic guidance, and outcome assessment in many clinical applications, such as wound healing, cancer surgery, and organ transplantation. Traditionally, structural characteristics of a wound tissue can be measured with a standard phantom or a transparent paper, which are invasive and inconvenient[1]. Optical techniques are non-invasive, rapid, and quantitative for characterizing tissue topography, which include multi-view imaging and optical coherence tomography (OCT) [2], etc. Multi-view images utilize multiple viewpoints and captured multiple pictures of objective tissue. With a three-dimensional reconstruction algorithm, the topography of the tissue can be obtained. OCT technique can be used to obtain depth information of the tissue. With a penetration depth up to 3 mm, OCT has been used in the skin disease diagnosis [3-5]. Functional characteristics are very important for accurate and quantitative assessment of tissue disorder, such as wound, cancer, and transplantation organ. Tissue oxygenation, perfusion, vascular, and inflammation are all important functional factors to assess tissue status, which is useful for further therapy. Hyperspectral imaging, laser speckle imaging, laser Doppler imaging, and thermographic imaging are effective techniques to acquire tissue oxygenation map, tissue vascular, blood perfusion, and heat emission characteristics of tissue[6-9], some of the techniques have been applied in clinical treatment. However, many clinical imaging systems have limitations and fail to provide noninvasive, real time, and quantitative assessment on structural and functional characteristics of biological tissue simultaneously in an operation room. To overcome these limitations, we developed and tested a multiview hyperspectral imaging system, which integrated the multiview and the hyperspectral imaging techniques in a single portable unit. Four plane mirrors were cohered together as a multiview reflective mirror set with a rectangular cross section. The multiview reflective mirror set was placed between a hyperspectral camera and the measured biological tissue. For a single image acquisition task, a hyperspectral data cube with five views was obtained. The five-view hyperspectral image consisted of a main objective image and four reflective

images. Three-dimensional topography of the scene was achieved by correlating the matching pixels between the objective image and the reflective images. Three-dimensional mapping of tissue oxygenation was achieved using a simple functional diffuse reflectance spectroscopy (fDRS) algorithm. In the algorithm, only four wave length spectroscopy, 530, 545, 570, and 584 nm were applied to obtain tissue oxygenation point by point, which can reduce scattering effects and melanin absorption [10]. Our multiview hyperspectral imaging technique is currently under quantitative validation in a wound model, a tissue-simulating blood phantom, and an in vivo biological tissue model. Our preliminary results have demonstrated the technical feasibility of using multiview hyperspectral imaging for three-dimensional topography of tissue functional properties.

2. MULTIVIEW HYPERSPECTRAL IMAGING SYSTEM

A multiview imaging system and a multispectral imaging system were integrated together to obtain the topographic and oxygenation characteristics of tissue. The integrated system is simple, cost-effective, and portable that can be easily used in clinical treatment.

2.1 Multi-viewpoint imaging

A multiview imaging system consists of a camera and a square mirror set. The square mirror set is composed of four plane mirrors that are cohered together with a square cross section. This configuration allows us to obtain five different views of the target within a single image at the exactly same time. With a 3-dimension reconstruction algorithm, the three dimensional superficial characteristics of the tissue can be obtained.

The basic principle underlying the multi-viewpoint imaging system is shown in Figure 1. The camera is placed on one side of the Square Mirror, and its optical axis is coincident with the axis of the square mirror. Each of the four mirrors around produces a virtual camera with the same camera parameters on the other side. Thus the virtual cameras are symmetric with respect to the optical axis, and the distance between a real camera and a virtual camera is equal to that between the opposite mirrors. The five “cameras” will take pictures of Point P from different viewpoints. As a result, three-dimensional topography of the scene can be achieved by correlating the matching pixels between the objective image and the reflective images.

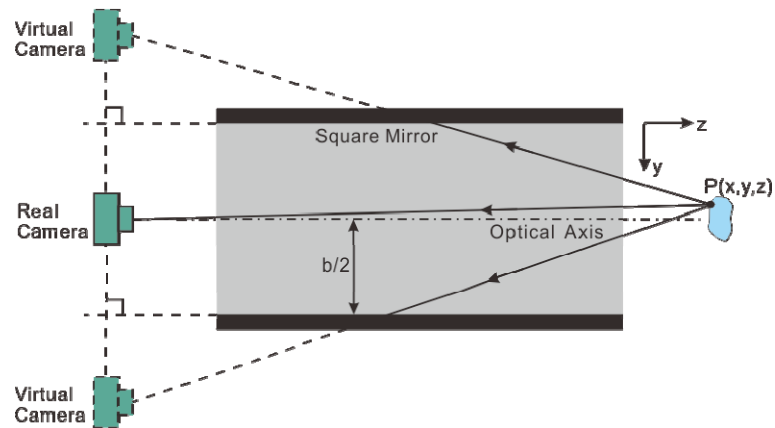


Fig. 1 Principle of the multi-view imaging system

After obtaining a multiview photography of the target, we need to cut and mirror the four images taken by the virtual cameras in order to carry out the correlation matching. Figure 2 gives an example of how to cut and mirror the right image. Assume that Point A and B' are matching points in the middle and right images respectively. After mirroring the photo horizontally, we transform Point B' in the original right image into Point B in the mirrored image.

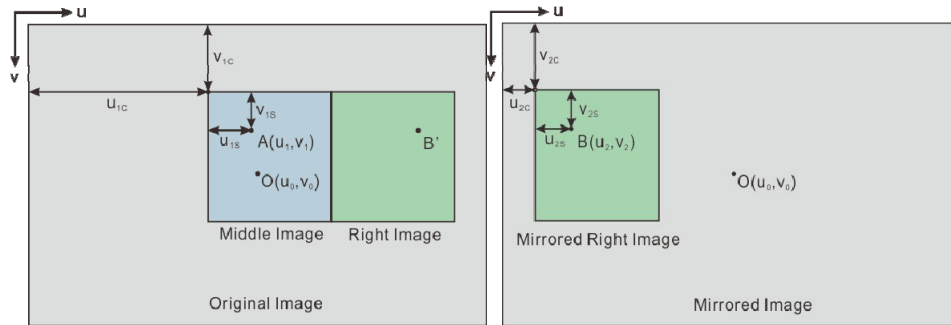


Fig. 2 Image cutting and mirroring

Assuming that the coordinate of A in the original image is (u_1, v_1) , the coordinate of B in the mirrored image is (u_2, v_2) , the coordinate of A in the middle image is (u_{1S}, v_{1S}) , the coordinate of B in the mirrored right image is (u_{2S}, v_{2S}) , the coordinate of the top left corner of the middle image is (u_{1C}, v_{1C}) , the coordinate of A the top left corner of the mirrored right image is (u_{2C}, v_{2C}) , the width of the original image and middle image is U_0 and $Column$, then we get the transformation of coordinates

$$\begin{cases} u_1 = u_{1C} + u_{1S} \\ v_1 = v_{1C} + v_{1S} \end{cases} \quad \begin{cases} u_2 = u_{2C} + u_{2S} \\ v_2 = v_{2C} + v_{2S} \end{cases} \quad (1)$$

$$U_0 = u_{1C} + u_{2C} + 2Column \quad (2)$$

2.2 3D reconstruction

As shown in Figure 1, Point $P(x, y, z)$ is on the target object. It can be projected on the images taken by the real and virtual cameras as Point $A(u_1, v_1)$ and $B(u_2, v_2)$. As the parameters of the real and virtual cameras are exactly the same and their optical axis are parallel, x, y and z can be described like

$$\begin{cases} x = \frac{b(u_1 - u_0)}{u_1 - u_2} \\ y = \frac{b\alpha_x(v_1 - v_0)}{\alpha_y(u_1 - u_2)} \\ z = \frac{b\alpha_x}{u_1 - u_2} \end{cases} \quad (3)$$

where b is the distance between real and virtual cameras, (u_0, v_0) denotes the center of the original image, shown in Figure 1. α_x, α_y, u_0 and v_0 are the parameters of the camera, which can be obtained through camera calibration. Especially, $u_1 - u_2$ is often called *disparity*, and in this case,

$$disparity = u_1 - u_2 = 2u_{1C} - U_0 + 2Column + (u_{1S} - u_{2S}) \quad (4)$$

Therefore, (x, y, z) can be written as

$$\begin{cases} x = \frac{b(u_{1C} + u_{1S} - u_0)}{2u_{1C} - U_0 + 2Column + (u_{1S} - u_{2S})} \\ y = \frac{b\alpha_x(v_{1C} + v_{1S} - v_0)}{\alpha_y[2u_{1C} - U_0 + 2Column + (u_{1S} - u_{2S})]} \\ z = \frac{b\alpha_x}{2u_{1C} - U_0 + 2Column + (u_{1S} - u_{2S})} \end{cases} \quad (5)$$

For convenience, we define a new parameter, the *disparity'*, in the following equation,

$$disparity' = u_{1S} - u_{2S} \quad (6)$$

where *disparity'* is the result of the correlation matching between the middle and mirrored right images. As we can see from Equations 5 and 6, the 3D coordinates (x,y,z) of a point on the object is relevant to its *disparity'* that is obtained from the correlation matching.

In the matching process, when obtaining *disparity'*, we used a local and window-based method for stereo matching that is based on normalized cross-correlation (NCC)[11]. Incorporating sub-pixel[12] computation into the matching matrix to avoid the contouring effects caused by integer-valued disparity estimates, and detecting the occluded areas using cross-checking[13], we have greatly refined the accuracy of the disparity estimates.

2.3 Multiview imaging system

With a multiview reflective mirror set between the camera and objective tissue, a multiview imaging system can be set up to obtain the three dimensional topography of the objective tissue. Furthermore, if the imaging system captures the hyperspectral images of the objective tissue, the functional characteristics such as oxygen saturation of the objective tissue can be calculated. Finally, the three dimensional topography with the functional characteristics of the tissue can be obtained immediately and conveniently.

In order to obtain the hyperspectral images of the objective tissue, OL 490-VIS (Optronic Laboratories Llc) was used as the light source that provide a wide wavelength range [500~900] nm at a spectral resolution of 2 nm. A light ring is connected to the tunable light source to provide a uniform illumination. After obtaining the hyperspectral images of the objective tissue, a simple functional diffuse reflectance spectroscopy (fDRS) algorithm was used to remove the effect of scattering and melanin absorption, and reconstruct tissue oxygenation maps based on hyperspectral images [10].

3. EXPERIMENTAL VALIDATION OF THE SYSTEM

Our multiview hyperspectral imaging techniques are currently under quantitative validation in a wound model, a tissue-simulating blood phantom, and an in vivo biological tissue model. Our preliminary results have demonstrated the technical feasibility of using multiview hyperspectral imaging for three-dimensional topography of tissue functional properties.

3.1 Multiview imaging of wound model

A wound model (as shown in Figures 3 (c) (d)) with four chronic wounds that represent different phases of the pressure-induced chronic wound was used in the experiment to validate the multiview imaging system. A canon 5D mark II camera with EF 24-105mm lens was used to capture the multiview photography of the wound model. One of the wounds was measured by the multiview imaging system (as shown in Figure 3 (a) (e)) and a coordinate measuring machine (Sheffield Measurement, CORDAX RS-30, as shown in Figure 3 (b)) respectively. With the algorithm described in the previous section, we could obtain the 3D morphology of the wound.

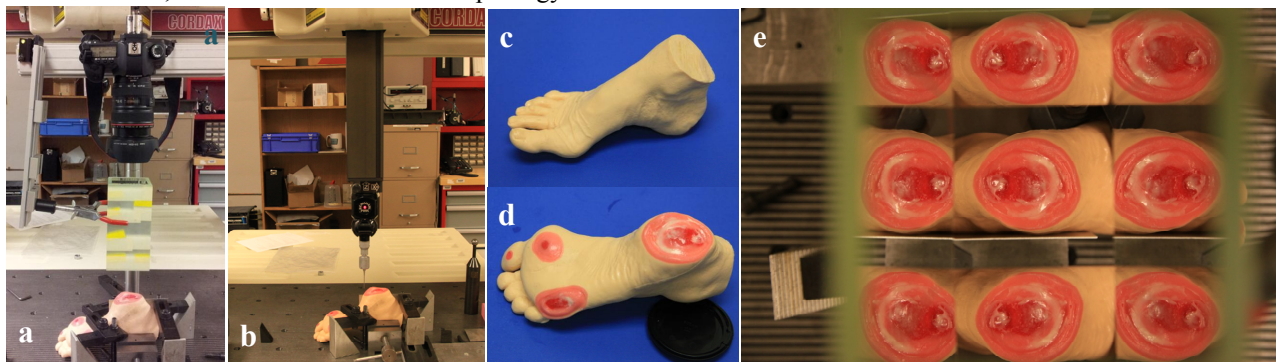


Fig.3 Multiview imaging for 3D reconstruction of the chronic wound model: (a) multiview imaging system for 3D reconstruction of the wound model; (b) CMM system for measuring the topography of the wound model; (c) the wound model; (d) four representative wounds on the wound model; (e) a photograph of the wound taken by the multiview imaging system.

Figure 4 displays the results of the multiview imaging system and CMM respectively. From the figures, we could conclude that 3D topography of the wound model that is obtained from the multi-view imaging system is very close to that of the CMM system, which also validate the multiview imaging system preliminarily.

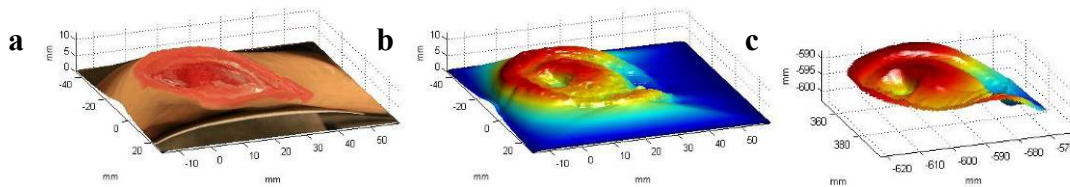


Fig. 4 (a) Topography of the wound model obtained from the multi-view system; (b) topography of the wound model obtained from the multi-view system; (c) topography of the wound model obtained from CMM.

3.2 Multi-view hyperspectral imaging of a tissue-simulating blood phantom

Another experiment was conducted to combine the multi-view imaging and the hyperspectral imaging together. The experimental setup is displayed in Figure 5 (a). The multi-view hyperspectral system consists of a NIR high resolution camera, a multiview reflective mirror set, a tunable light source, a light ring, and a tissue-simulating blood phantom. A tissue-simulating blood phantom was put in a tube that was placed on a tilt in the view field of the multiview hyperspectral system to verify the performance of the system. With the multiview system, the topography of the tube was reconstructed as shown in Figure 5 (b), and the tissue oxygenation maps were calculated based on hyperspectral images. The followings are the steps to make a tissue-simulating blood phantom: (1) add 20 g milk powder into water and get 200 ml milk; (2) get a mixture of blood by mixing 200 ml milk, 70 ml water, and 12 ml blood of a healthy subject; (3) pour the mixture of blood into a tube with 60 ml volume; (4) add 1 g hydroxide into 40 ml water to get the sodium hydroxide. After one hyperspectral measurement, we can obtain the oxygenation of the simulating blood phantom. Then we use a syringe to get sodium hydroxide and slowly inject it into the tube. Thus a new recipe of the blood phantom with a decreased oxygenation was prepared for a new measurement by the multiview hyperspectral imager. For each recipe, the volume of the sodium hydroxide that be injected in the tube is 0, 0.1, 0.15, 0.15, 0.20, 0.25, and 0.30 ml respectively.

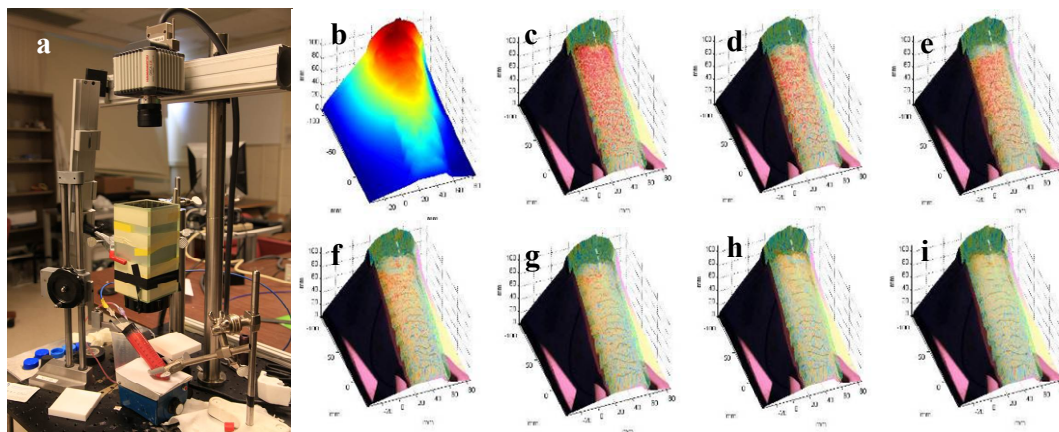


Fig. 5 Multiview hyperspectral imaging of a tissue-simulating blood phantom: (a) experimental setup; (b) topography of the tube; (c)~(i) topographic oxygenation map of the tissue-simulating blood phantom from recipe 1 to 7, red color denotes a higher oxygen saturation, while blue color denotes a lower oxygen saturation.

Figures 5 (c) ~ (i) display oxygenation maps of the tissue-simulating blood phantom with the topography characteristics. From the figure, it can be easily obtained that the oxygen saturation of the blood phantom decreases along with the volume of the sodium hydroxide increasing. The result indicates that the structural and functional characteristics of the simulated blood phantom can be easily achieved with the simple multiview hyperspectral system.

3.3 Multi-view hyperspectral imaging of an *in vivo* tissue model

An *in vivo* experiment was also designed to verify the integrated multiview hyperspectral system. A healthy subject's fingers were put in the view field of the integrated system, and an occlusion experiment was conducted, in which the fingers were continuously monitored from the beginning of the occlusion to the post occlusive reactive hyperaemia. Before the experiment, a pressure cuff was applied around the upper arm of the subject. Then we began to monitor the tissue structural and functional characteristics with the multiview hyperspectral imaging system simultaneously. After 1 minute baseline measurement, an occlusion was created with the pressure cuff. We inflated the cuff quickly above 180 mm/Hg and maintained the pressure for another 2 minutes, which was called as occlusion stage. After that, the cuff was released and a reactive hyperaemia emerged at the beginning of the reperfusion stage. The dynamics of three dimensional oxygen saturation maps of the fingers could be obtained from the analysis on the data from the multiview hyperspectral imaging system.

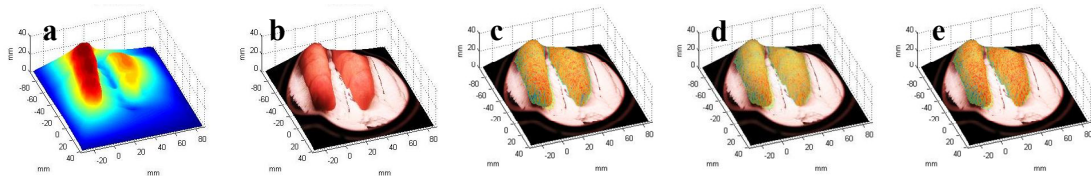


Fig. 7 Multiview hyperspectral imaging of a healthy subject's fingers in an occlusion experiment: (a) 3D topography of the fingers; (b) 3D topography of the fingers with texture; (c) 3D oxygenation distribution of the fingers at one moment during the baseline stage; (d) 3D oxygenation distribution of the fingers at one moment during the occlusion stage; (e) 3D oxygenation distribution of the fingers at one moment during the reperfusion stage.

Figure 7 displays the result of the occlusion experiment on the healthy subject. Figure 7 (a) is the topography of the fingers, while Figure 7 (b) is the textured topography of the fingers. Figures 7 (c), (d), (e) are topography of the fingers with oxygenation characteristics at one moment during the baseline, occlusion, and reperfusion stage respectively. The result indicates the occlusion effect and hyperaemia effect clearly, which also implies that the system can obtain topographic and oxygenation characteristics simultaneously in live tissue.

4. CONCLUSION

A multiview hyperspectral imaging system was developed to map the three-dimensional oxygenation distribution on biological tissue. A multiview reflective mirror is placed in front of the lens of the hyperspectral imager, and the topography of tissue with oxygenation map could be obtained with a three-dimension reconstruction algorithm and a wide gap second derivative spectroscopic algorithm. The imaging system is simple, portable, noninvasive, cost effective, and clinically implementable for applications such as wound healing assessment, intraoperative surgical navigation, and organ transplantation. Three experiments were conducted to validate the system. A wound model was imaged by the integrated system and a CMM system respectively, the results from the multiview imaging system and the CMM system are in accordance which verified the model preliminarily. A tissue-simulating blood phantom and an *in vivo* experiment were also conducted and the results also indicate that the integrated system can achieve the structural and functional characteristics of the tissue simultaneously. Our preliminary results have demonstrated the technical feasibility of using multiview hyperspectral imaging for three-dimensional topography of tissue functional properties, which is very useful for clinical treatment. The future work will mainly concern the calibration of the multiview imaging and hyperspectral imaging system.

ACKNOWLEDGMENT

This research is sponsored by National Institute of Standards and Technology (60NANB10D184), US Army Medical Research Acquisition Act (W81XWH-11-2-0142) and National Science Foundation of China (81271527).

REFERENCES

- [1] Ahn, C. and Salcido, R. S., "Advances in wound photography and assessment methods," *Adv Skin Wound Care*, 21 (2), 85-93, (2008).
- [2] Fercher, A. F., "Optical coherence tomography," *Journal of Biomedical Optics*, 1 (2), 157-173, (1996).
- [3] Pierce, M. C., Strasswimmer, J., Park, B. H., Cense, B., and de Boer, J. F., "Advances in optical coherence tomography imaging for dermatology," *Journal of Investigative Dermatology*, 123 (3), 458-463, (2004).
- [4] Gladkova, N. D., Petrova, G. A., Nikulin, N. K., Radenska - Lopovok, S. G., Snopova, L. B., Chumakov, Y. P., Nasonova, V. A., Gelikonov, V. M., Gelikonov, G. V., and Kuranov, R. V., "In vivo optical coherence tomography imaging of human skin: norm and pathology," *Skin Research and Technology*, 6 (1), 6-16, (2000).
- [5] Welzel, J., Lankenau, E., Birngruber, R., and Engelhardt, R., "Optical coherence tomography of the human skin," *J Am Acad Dermatol*, 37 (6), 958-963, (1997).
- [6] Kellicut, D. C., Weiswasser, J. M., Arora, S., Freeman, J. E., Lew, R. A., Shuman, C., Mansfield, J. R., and Sidawy, A. N., "Emerging technology: hyperspectral imaging," *Perspectives in vascular surgery and endovascular therapy*, 16 (1), 53-57, (2004).
- [7] Nilsson, G. E., Tenland, T., and Oberg, P. A., "Evaluation of a laser Doppler flowmeter for measurement of tissue blood flow," *IEEE Transactions on Biomedical Engineering*, (10), 597-604, (1980).
- [8] Kim, K., Huang, S. W., Ashkenazi, S., Odonnell, M., Agarwal, A., Kotov, N. A., Denny, M. F., and Kaplan, M. J., "Photoacoustic imaging of early inflammatory response using gold nanorods," *Applied Physics Letters*, 90 (22), 223901, (2007).
- [9] Kirkpatrick, S. J. and Cipolla, M. J., "Laser speckle microstrain measurements in vascular tissue," in *Proc. SPIE*, 1999, pp. 121-129.
- [10] InSeok Seo, P. R. B., and Nikiforos Kollias, "Simultaneous assessment of pulsating and total blood in inflammatory skin lesions using functional diffuse reflectance spectroscopy in the visible range," *Journal of Biomedical Optics*, 15 (6), 060507-1.
- [11] Scharstein, D. and Szeliski, R., "A taxonomy and evaluation of dense two-frame stereo correspondence algorithms," *Int J Comput Vis*, 47 (1), 7-42, (2002).
- [12] Ryan, T., Gray, R., and Hunt, B., "Prediction of correlation errors in stereo-pair images," *Optical Engineering*, 19 (3), 193312, (1980).
- [13] Fua, P., "A parallel stereo algorithm that produces dense depth maps and preserves image features," *Machine vision and applications*, 6 (1), 35-49, (1993).